NASA TN D-441

TECHNICAL NOTE

D-441

FLIGHT PERFORMANCE OF A SPIN-STABILIZED 20-INCH-DIAMETER SOLID-PROPELLANT SPHERICAL ROCKET MOTOR

By Jack Levine, C. William Martz, Robert L. Swain, and Andrew G. Swanson

Langley Research Center
Langley Field, Va.

NATIONAL AERONAUTICS AND SPACE ADMINISTRATION

WASHINGTON

September 1960

L

NATIONAL AERONAUTICS AND SPACE ADMINISTRATION

TECHNICAL NOTE D-441

FLIGHT PERFORMANCE OF A SPIN-STABILIZED 20-INCH-DIAMETER SOLID-PROPELLANT SPHERICAL ROCKET MOTOR

By Jack Levine, C. William Martz, Robert L. Swain, and Andrew G. Swanson

SUMMARY

A successful flight test of a spin-stabilized 20-inch-diameter solid-propellant rocket motor having a propellant mass fraction of 0.92 has been made. The motor was fired at altitude after being boosted by a three-stage test vehicle. Analysis of the data indicates that a total impulse of 44,243 pound-second with a propellant specific impulse of approximately 185 was achieved over a total action time of about 12 seconds. These results are shown to be in excellent agreement with data from ground static firing tests of these motors. The spherical rocket motor with an 11-pound payload attained a velocity of 15,620 feet per second (M = 16.7) with an incremental velocity increase for the spherical motor stage of 12,120 feet per second.

INTRODUCTION

The use of rocket vehicles as tools in conducting hypersonic free-flight research requires high-performance rocket motors, particularly in the latter stages of multistage vehicles. If these latter stages operate at high altitude, drag and other aerodynamic considerations are minimized and prime emphasis can be placed on achievement of high mass ratios and overall rocket-motor specific impulse.

Solid-propellant spherical rocket motors offer significant advantages over conventional cylindrical motors for high-altitude operation. The use of the highly efficient spherical pressure vessel as a rocket-motor case results in a substantial reduction in rocket-motor case weight and enables high mass ratios to be obtained. The Langley Research Center is currently conducting research on spherical rocket motors of various diameters through a series of ground and flight tests.

Some of the results of this program are reported in references 1 and 2, which present results of the ground static firing of three 10-inch-diameter spherical rocket motors and the free-flight tests of two 10-inch-diameter spherical rocket motors.

Reported herein are the results of a ground static test and a flight test of 20-inch-diameter solid-propellant spherical rocket motors. The purpose of the present investigation was to evaluate, under actual missile environment, the performance of the spherical rocket motor in free flight at high-altitude conditions. The ground test was conducted at the Langley Research Center. The flight test was made at the NASA Wallops Station.

A multistage solid-propellant rocket system was employed to boost the spherical motor to altitude for the flight test. The spin velocities required for stabilization of the spherical rocket stage were obtained by aerodynamic means through canting of the previous-stage stabilizing fins. An analysis of the spin-up motion and sphere stabilization prepared by C. William Martz is presented in the appendix.

SYMBOLS

a_n	normal acceleration, ft/sec^2
a_l	longitudinal acceleration, ft/sec^2
a_t	transverse acceleration, ft/sec^2
A	frontal area, sq ft
A_t	nozzle throat area, sq in.
C^*	characteristic velocity (propellant performance parameter), ft/sec
C_D	drag coefficient
C_w	nozzle discharge coefficient, sec^{-1}
g	gravitational constant, 32.2 ft/sec^2
I_{sp}	propellant specific impulse, I_T/W_p, lb-sec/lb
I_T	total impulse, $\int T\,dt$, lb-sec
$\dot{m}$	weight discharge rate, lb/sec
M	Mach number
p_c	chamber pressure, lb/sq in. abs

q	dynamic pressure, lb/sq ft
R	Reynolds number
t	time, sec
T	thrust, lb
V	velocity, ft/sec
ΔV	incremental velocity increase, ft/sec
W	weight, lb
γ	flight-path angle, deg
α	angle of attack, deg

Subscripts

∞	free-stream conditions
e	empty
l	loaded
P	propellant
T	total
PC	propellant consumed
PR	propellant remaining

MOTOR DESIGN

The flight-tested spherical rocket motor was one of two identical 20-inch-diameter motors fabricated in the Langley Research Center and loaded with propellant by the Thiokol Chemical Corporation (Elkton Division). The cases were machined in two hemispheres from SAE 4130 steel which had been heat treated to a minimum yield strength of 150,000 pounds per square inch Rockwell C-36 hardness. The wall thickness of the case was 0.032 ± 0.002 inch and the case was designed for an operating chamber pressure of 600 pounds per square inch. This measurement was increased to 0.090 inch in the area where the forward and rearward hemispheres were joined by welding. No post-welding, heat-treating

operation was possible because of the method of installation of the mandrel to form the propellant-grain configuration. A threaded boss of 3.6 inches diameter was machined into the forward end of the case to provide mounting for a radar transponder assembly. The extreme rear of the case was thickened to permit machining of threads for nozzle mounting. The welded empty case weighed 18 pounds.

The rocket-motor nozzle was machined from SAE 4130 steel. The throat insert was AGX graphite backed by eight layers of a phenolic-fiberglass laminate liner which extended down the divergent nozzle cone to the nozzle exit. The total thickness of this liner was 0.080 inch. Initial flight vehicle design utilized the nozzle of the 20-inch-diameter spherical motor as the primary structural support member for that motor and the payload and thus dictated a fairly short nozzle. Nozzle studies indicated that the overall performance of the vehicle would not decrease appreciably with the short nozzle. The nozzle was therefore shortened for structural mounting purposes to an expansion area ratio of 3.6, and thus yielded an underexpanded exhaust-gas flow system. The nozzle design was not altered when the vehicle design was modified to support the spherical motor in a foamed plastic cradle. The throat was machined to yield an average operating chamber pressure of 600 pounds per square inch for a propellant temperature of 70° F. The total nozzle weight was 3.0 pounds. Figure 1(a) is a sketch of the motor case and nozzle.

The propellant employed was T-22, a polysulfide-perchlorate composite, the properties of which may be found in reference 3. At the time of loading the 20-inch spherical motors by Thiokol, small test motors were cast from the same propellant mix to determine the ballistic performance for that particular propellant mix. These ballistic data showed a characteristic exhaust velocity C^* of 4,460 feet per second at a pressure of 1,000 pounds per square inch for the propellant within the 20-inch motors. The total propellant weight was 239 pounds.

The propellant configuration and method of manufacture was the same as presented in reference 1. The technique of employing a grain form of a low-melting-temperature eutectic alloy about which the propellant is cast and oven cured was used. The alloy grain form was subsequently removed from the cured motor by elevating the oven temperature above that required to melt the alloy form. Figures 1(b) and 1(c) show the propellant-grain configuration.

The igniter for the 20-inch-diameter spherical rocket motor was designed and fabricated at the Langley Research Center. Experience at Langley in igniting 5-inch- and 10-inch-diameter spherical rocket motors had shown the igniter to be most effective when located in the outer periphery of the semicircular slots of the propellant port configuration. Fifteen grams (0.033 lb) of U.S. Flare 2A boron pellets contained in a thin frangible plastic tube were inserted in each slot along with a squib.

Thirty-five grams (0.077 lb) of U.S. Flare 2A boron pellets were contained at the forward end of a larger thin cellulose acetate tube down the motor axis. This tube contained three squibs. A total of 10 instantaneous squibs, wired for a 3-wire ignition circuit was used. The total weight of igniter pyrotechnic was 140 grams (0.308 lb). Location of the igniter components is shown in figures 1(b) and 1(c).

STATIC-TEST FIRING RESULTS

The first of the two 20-inch-diameter spherical rocket motors manufactured was static-test fired at the Langley Research Center. The motor was mounted in a contoured carriage which permitted motor growth while under internal pressure. The carriage was mounted on rollers to permit thrust measurement. Pressure taps were not incorporated into the flight motor case design. All rocket components, including the igniter, were of the same type subsequently used in the flight test. Excellent ignition was obtained.

The thrust-time trace was satisfactory until 7.2 seconds at which time a case burn-through occurred in the rear hemisphere of the case, slightly above the nozzle attachment. The anticipated burning time to web burnout was 8.1 seconds with a total action time of 12 seconds. The case burn-through was not surprising since X-rays of the motor at the manufacturers showed a splinter of wood 5 inches long imbedded at the exact area of the failure. The origin of this splinter was never determined. It is believed that this splinter which protruded into the combustion zone provided a path for the hot combustion gases to reach the case wall prematurely. A visual inspection of the case after firing showed that, aside from the burn-through location, the remainder of the case and nozzle were in excellent condition. In view of the known flaw in the first 20-inch-diameter spherical rocket motor, the static-firing ground test was considered to be successful and it was therefore believed that a second static firing would not be required prior to flight test of this design.

The thrust-time history from the static firing of the first 20-inch-diameter spherical motor was used as the basis for a trajectory calculation for the flight vehicle. The measured thrust-time trace was employed as such for the first 7.2 seconds of motor burning. The remainder of the trace was calculated from propellant internal port configuration design and the experimental results of ground static firings of 5-inch and 10-inch spherical motors of the same internal configuration. The thrust-time trace was then corrected to altitude firing conditions with an average ambient pressure assumed of 1 pound per square foot. The anticipated web burning time remained 8.1 seconds with a total action time of 12 seconds.

The experimental results of three ground static firings of 10-inch-diameter spherical rocket motors are presented in reference 1. For those particular tests reported, the propellant was T-21, a polysulfide-perchlorate composite, whose properties are found in reference 3. Theoretically, T-22 propellant, as used in the 20-inch spherical rocket motors reported herein, has a slightly higher specific impulse than T-21 at comparable pressures (ref. 3). It was therefore decided to employ T-22 as the propellant for subsequent tests of 5-inch and 10-inch spherical rocket motors cast at the Langley Research Center. If a typical value for nozzle efficiency of 0.97 was used in both instances, near theoretical performance was achieved with the T-21 propellant in the spherical motor design whereas the T-22 propellant failed to develop theoretical performance by a large margin. Unpublished results of the static firings of five 5-inch-diameter spherical rocket motors and one 10-inch-diameter spherical rocket motor, all motors containing T-22 in the propellant configuration of reference 1, demonstrated delivered propellant specific impulses for T-22 of from 8.5 percent to 11.5 percent below the theoretical specific impulse. This phenomenon has later been found to exist with other propellants in the cited and similar internal port configurations and is felt to be a function of propellant composition as affecting the "dwell" or "residence" time of the propellant exhaust gases within the spherical motor. The extremely short spherical rocket motor chamber does not allow the propellant gases, from certain propellant compositions, to develop full impulse before being ejected through the rocket nozzle. Further discussion of this phenomenon is beyond the scope of this report.

L 9 5 6

For purposes of estimating a realistic flight trajectory, the delivered propellant specific impulse from the measured ground static firing of the first 20-inch-diameter spherical rocket motor was calculated from a fairing of the curve as previously discussed. This propellant specific impulse was 11.0 percent below that obtained from the test motors containing this T-22 propellant fired by Thiokol as discussed under Motor Design. When corrected to altitude conditions, this propellant specific impulse was 190.5 lb-sec/lb for the period up to web burnout and 184.0 lb-sec/lb over the total action time of 12 seconds. The anticipated total impulse was 44,000 lb-sec. This value yielded an anticipated ΔV for the spherical rocket motor stage of 12,320 ft/sec, an 11-pound payload being assumed.

The poor performance of the T-22 propellant in the spherical motors was reflected by an increase in the propellant discharge coefficient from 0.00733 sec^{-1} as determined by the previously discussed Thiokol test motors to 0.00825 sec^{-1} for the actual delivered performance in the 20-inch spherical motor ground static firing test. The propellant discharge coefficient C_w, is a parameter measuring the performance of a propellant; the lower the coefficient, the higher the performance. This coefficient relates the rocket weight discharge rate $\dot{m}$, the chamber

pressure p_c, and the nozzle throat area A_t by the following equation

$$C_w = \frac{\dot{m}}{A_t p_c} \tag{1}$$

The variation of the weight of propellant remaining within the motor as a function of motor burning time was calculated stepwise from a calculated pressure time history. A nozzle throat, negligible erosion during burning being assumed, of 6.61 square inches and a propellant discharge coefficient of 0.00825 sec^{-1} were used. The product of chamber pressure, throat area, and discharge coefficient yielded a weight discharge rate. By dividing the burning period into increments and stepwise subtracting the weight discharge over one increment from the propellant weight remaining immediately preceding that increment, the variation of weight of propellant remaining with time was obtained.

The design operating chamber pressure for both the static and the flight 20-inch-diameter spherical rocket motors was 600 pounds per square inch. However, because of the increase in the propellant discharge coefficient as mentioned above, the measured chamber pressure in the static firing was lower than design and averaged about 500 pounds per square inch. The 20-inch spherical rocket motor used in the flight test passed the X-ray examination satisfactorily.

FLIGHT-TEST VEHICLE SYSTEM

Spherical Rocket Stage

The 20-inch-diameter spherical rocket motor tested in this flight comprised part of the fourth stage of the vehicle system. A heat shield was employed to protect the spherical motor from aerodynamic heating effects during boost and at the high velocities attained during thrusting. A radar transponder was attached to the front of the motor to aid in determining the flight trajectory. The general arrangement of the spherical rocket motor, heat shield, and radar transponder is shown in figures 1(d) to 1(f).

The brackets, in which the beacon antenna was inserted, were bonded with Epoxy cement to the motor case diametrically opposite each other. Tunnels for the antenna leads were located under the heat shield and were bonded to the motor case. Figure 1(e) is a photograph showing the transponder and antenna assembly on the motor prior to installation of the heat shield. The antenna brackets were protected from aerodynamic heating by an 0.04-inch-thick Inconel strip attached to the heat shield as shown in figure 1(f).

Figure 2 shows the arrangement of the spherical rocket motor mounted to the third-stage booster. A threaded blowout diaphragm coupled the spherical motor nozzle to the adapter forward of the third-stage booster. Foamed plastic was molded to form a cushioned cradle or seat for the rocket motor within the booster adapter.

A photograph of the complete test vehicle in launch position is shown as figure 3. The first stage of this system was an M6 JATO rocket motor (Honest John); the second and third stages were each an M5 JATO rocket motor (Nike).

Trajectory Flight Plan

The complete vehicle system, the 20-inch-diameter spherical rocket motor and three boost stages, weighed 6,980 pounds and was launched at an elevation angle of 78°. The first three stages, fired in delayed sequence, propelled the spherical rocket motor along a nominal zero lift trajectory as shown in figure 4.

The firing and coast sequence for the various stages was chosen to obtain the maximum velocity at the firing altitude for the spherical motor without exceeding allowable skin temperatures. During coasting flight, premature separation of later stages was prevented by locking devices between the second, third, and fourth stages. The second- and third-stage motors were fired by delay squibs ignited at launching of the vehicle. The spherical rocket motor containing zero delay or instantaneous squibs was ignited by a preset mechanical timer which was actuated by an inertia switch at launching. Disengagement of the lock mechanism between the second and third stages was accomplished by a delay squib. A blowout diaphragm coupled the third and fourth stages and was ruptured by the ignition blast of the fourth-stage spherical rocket motor.

As noted in figure 2, the third-stage fins were canted 1°; this canting imparted a sufficient spinning motion to this stage to spin-stabilize the spherical motor stage without employing additional hardware. This technique is discussed in detail in the appendix.

Instrumentation

A four-channel telemeter was mounted on the forward end of the third-stage motor as shown in figure 2. Measurements were transmitted during the flight from four accelerometers of longitudinal, normal, and transverse accelerations. Accelerometer full-scale ranges were:

Low-range longitudinal accelerometer	1g (thrust) to -6g (drag)
High-range longitudinal accelerometer . . .	45g (thrust) to -6g (drag)
Normal accelerometer	±25g
Transverse accelerometer	±25g

The longitudinal accelerometers were included to indicate the time of sphere ignition and to provide velocity information up to that time. The normal and transverse accelerometers were employed to detect flight irregularities during the boost portion of the flight. The telemeter antenna spikes were mounted on the forward end of the third stage as shown in figure 2. A determination of the vehicle roll rate was made from the variations in telemeter signal strength received from this polarized antenna.

A AN/DPN-19 radar transponder was mounted to the front end of the spherical rocket motor to aid in tracking this stage with the Reeves modified SCR-584 radar. Unfortunately, the transponder failed at about 48 seconds after launch, some 17 seconds before spherical motor ignition. However, the spherical rocket stage was skin-tracked with an FPS-16 tracking radar to an altitude of approximately 100 miles. Data were also obtained by the Millstone Hill experimental radar of the M.I.T. Lincoln Laboratory for that part of the trajectory above an altitude of approximately 160 miles. The vehicle system was also tracked by a CW Doppler velocimeter which obtained velocity data through burnout of the second booster stage. Atmospheric and wind conditions were determined by means of a radiosonde launched near the time of flight and tracked by a Rawin set AN/GMD-1A to an altitude of 120,000 feet.

FLIGHT-TEST RESULTS

Trajectory Through Spherical Motor Burnout

Figures 5(a) and 5(b) show the flight velocity time history. Time histories of free-stream Mach number and Reynolds number per foot are shown in figure 6. The velocity time history was determined from data obtained by a CW Doppler radar unit until shortly before third-stage ignition ($\approx$ 28 seconds); from then until sphere burnout, velocity was determined from differentiation of the space-position radar data.

The ignition time of the spherical rocket motor was determined from accelerometers located forward on the third-stage booster. The exact time of the spherical motor ignition could not be accurately determined from the radar data because of the relatively slow change in range of the spherical motor stage. This slow change in range also made it difficult to determine with extreme accuracy the velocity for the first 2 seconds of sperical motor burning. A variation from the data presented of about $\pm$100 feet per second during this period is believed to represent the accuracy band within which the velocity could be determined from the differentiation of the space-position radar data. Since the burning of the spherical motor was confined to high-altitude conditions of relatively negligible aerodynamic drag, it decelerated very slowly at burnout. This

made it difficult to determine with extreme accuracy the maximum velocity and time of burnout from the radar data. The maximum velocity data are believed to be accurate to within about ±250 feet per second and the time of the spherical motor burnout is deemed to be accurate with ±1/2 second.

The data of figure 5(b) indicate that the spherical rocket motor attained a maximum velocity of approximately 15,620 feet per second (M = 16.7) with an incremental velocity increase ΔV for the spherical stage of about 12,120 feet per second.

Trajectory After Spherical Motor Burnout

The FPS-16 space-position radar located at the NASA Wallops Station tracked the spherical rocket stage to an altitude of 550,000 feet. The Millstone Hill experimental radar of M.I.T. Lincoln Laboratory was able to track this stage from approximately 850,000 feet altitude until about 3,500,000 feet. After this time the return signal became weak and approached the noise level of the receiver. Data received subsequent to this time scattered about a nominal flight path.

By using the velocity, altitude, and flight-path angle at burnout of the spherical motor as obtained from the FPS-16 radar data, a computation was made on an IBM 704 electronic data processing machine to extend the flight-path data. This calculated flight path agreed extremely well with that determined from the Millstone Hill radar data up to an altitude of approximately 3.6×10^6 feet as shown in figure 7. It can be seen in this figure that beyond this point the scatter of the radar data makes it difficult to determine any other points to any degree of accuracy, before or after apogee. The total flight time was approximately 25 minutes.

Determination of Spherical Motor Flight Performance

The thrust of the flight 20-inch-diameter spherical rocket motor at any time t was determined by the basic equation:

$$T = \left[\frac{W\left(a_l + g \sin \gamma\right)}{g} + qAC_{D_T}\right]\frac{1}{\cos \alpha} \qquad (2)$$

The longitudinal acceleration a_l is shown in figure 8 and was obtained from the second differentiation of the range data as obtained by the FPS-16 radar set.

A total drag coefficient C_{D_T} of 1 was assumed for the spherical motor during its firing. Modified Newtonian theory predicts a value of C_{D_T} of 1.2 for a hemisphere in a supersonic flow regime. The value of C_{D_T} for the spike on sphere configuration would be expected to be somewhat lower. Furthermore, the effect of a 100-percent error in C_{D_T} on the computed motor performance would be negligible because of the very low dynamic pressure which exists. Also, it should be noted that α was very small as is shown in the appendix.

The variation of the weight of propellant remaining in the motor as a function of motor burning time was calculated stepwise from the calculated flight thrust time history by using the following relationship:

$$(W)_{PR} = (W)_P - (W)_{PC} = W_P - W_P \frac{I_t}{I_T} \tag{3}$$

The propellant weight at ignition of the flight spherical rocket motor was 239 pounds. The total impulse I_T was computed by integrating the flight thrust time trace, and the impulse at any time I_t was obtained by integrating the thrust over that period of time. Then I_t was divided by I_T which yielded the percentage of the total impulse consumed during this time and this value is also the percentage of the propellant consumed. Therefore, the amount of propellant consumed over this period of time is the product of the total propellant times the ratio of I_t/I_T. Thus the propellant remaining in the motor is simply the total propellant weight W_P minus the amount of propellant consumed W_{PC}. By dividing the burning period into increments and stepwise subtracting the weight consumed (discharged) over one increment from the propellant weight remaining immediately preceding that increment, the variation of weight of propellant remaining with time was obtained. Equation (2) was then used to compute a new thrust time history based on this new variation of propellant weight with time. This iterative procedure was repeated until the thrust and propellant variations with time were consistent. These final computed variations of thrust and weight are shown in figure 9.

It should be noted that there is reasonable doubt as to the actual values of the computed thrust for the first 2 seconds of motor burning as the value of a_l used in equation (2) was obtained from a second differentiation of the basic trajectory data. Computations of reasonable variations to the basic trajectory data show that the values obtained for the first 2 seconds of motor thrusting can be considered to be accurate within ±25 percent. The computed values of thrust for the remainder of

the motor burning time are more discriminate in nature since the basic trajectory data at these times are fairly accurate. During this time period only a ±5-percent variation in thrust was found when reasonable variations of the basic data were employed.

COMPARISON OF FLIGHT- AND STATIC-TEST RESULTS

The anticipated motor performance (thrust, chamber pressure, and propellant-weight time histories) for the spherical rocket motor as determined from a static ground firing as previously discussed is shown in figure 9 as dashed lines. Also shown in this figure as solid lines are the computed thrust and propellant-weight time histories of the flight-tested spherical motor. The anticipated average motor thrust was 5,200 pounds; however, the actual flight average motor thrust was somewhat lower. The two thrust curves show some appreciable difference in their characteristics. It is believed that these differences in the shape of the curves may be associated with the varying burning characteristics between the static firing and the spinning flight motor. The weight curves also, of course, show variations between static firing and flight test since thrust and weight data from the flight test were derived simultaneously in the iterative process previously discussed.

L 9 5 6

The velocity increment attained by the spherical rocket motor in flight was approximately 200 feet per second lower than the 12,320 feet per second which was predicted by the ground test data previously presented. This difference is essentially negligible, particularly since the flight-test results for the spherical motor stage were determined from differentiation of the space-position radar data. (These velocity data are believed to be accurate within ±350 feet per second.)

The values of I_{sp} were predicted from the following equations:

$$I_{sp} = \frac{I_T}{W_l - W_e} \tag{4}$$

$$I_{sp} = \frac{\Delta V + g\,\Delta t \sin \gamma}{g \log_e \frac{W_l}{W_l - W_p}} \tag{5}$$

and were reasonably consistent when the measured values of I_T $\left(I_{sp} \approx 185\right)$ and ΔV $\left(I_{sp} \approx 181\right)$ are used. (Note that these equations

can be used since the drag impulse during spherical motor burning was negligible.) The I_{sp} computed from equation (5) by using an additional ΔV of 200 feet per second would be about 185. Hence, within the uncertainty of the data, the values of I_{sp} computed from the equations (4) and (5) are in agreement. The anticipated thrust-time curve shows a total impulse of 44,000 pound-second with an overall propellant specific impulse of 184 pound-second per pound. The computed thrust-time curve from the flight data yields a total impulse of 44,243 pound-second and a specific impulse of approximately 185 pound-second per pound. The total action time for the flight and ground tests was approximately 12 seconds.

The flight test and static-firing test results are therefore in excellent agreement from both a total impulse comparison and total action time.

The spherical-rocket-motor flight test is considered to be a successful proof test of this type of motor design. With increases in propellant specific impulse and refinements in the mechanical design of the case which are well within the current state of the art, the spherical rocket motor design has extremely favorable possibilities for future use in high-performance rocket vehicles.

CONCLUSION

A successful flight test of a spin-stabilized 20-inch-diameter solid-propellant rocket motor having a propellant mass fraction of 0.92 has been made. The motor was fired at altitude after being boosted by a three-stage test vehicle. Analysis of the data indicates that a total impulse of 44,243 pound-second with a propellant specific impulse of approximately 185 was achieved over a total action time of about 12 seconds. These results are shown to be in excellent agreement with data from ground static firing tests of these motors. The spherical-rocket-motor design concept offers considerable potential for application to future high-performance rocket vehicles.

Langley Research Center,
National Aeronautics and Space Administration,
Langley Field, Va., May 24, 1960.

APPENDIX

SPIN-UP ANALYSIS

Spin Stabilization

Whereas the first three stages of the four-stage configuration were stabilized about the flight path by fins, the last stage of the configuration (20-inch-diameter spherical rocket motor with a radar transponder) was stabilized in pitch and yaw by spinning it about a principal axis nearly coincident with its longitudinal geometric axis. Stabilizing fins could have been used on the last stage to prevent tumbling until the model rose above the effective atmosphere but they would have reduced the maximum velocity and would have been difficult to attach in an effective location. L 9 5 6

Preliminary spin-rate requirements were computed with the following expression:

$$p_{req} = \sqrt{\frac{2M_o}{\zeta_{max} I_x \left(1 - \frac{I_x}{I}\right)}}$$

where

p_{req} minimum spin rate required, radians/sec

M_o total overturning moment, $M_e{}^{i\lambda} + p^2\eta(I - I_x)$, ft-lb

λ relative angular direction of asymmetry moment M, radians

η angular deviation of principal axis to longitudinal geometric axis, radians

I pitch and yaw moments of inertia, slug-ft^2

I_x roll moment of inertia, slug-ft^2

ζ_{max} maximum absolute magnitude of ζ, radians unless otherwise noted

ζ complex angle of total yaw, $\beta + i\alpha$, radians unless otherwise noted

β angle of sideslip, nonrolling body axes, radians, deg

α angle of attack, nonrolling body axes, radians, deg

This formula assumes that residual motion and aerodynamic forces are negligible, that the model is spinning at a constant rate, and that model moments of inertia and forward velocity are constant. Also the expression is restricted to models having rolling mass symmetry and assumes that angular displacements and velocities about the pitch and yaw axes are small. However, in view of the design and planned trajectory of the last stage, this formula was considered to be adequate for preliminary calculation.

Under the assumption that thrust misalinement of the 20-inch-diameter spherical rocket motor could be as large as 0.2° and that it was desirable to restrain the maximum total yaw angle (ζ_{max}) to about 5°, the required spin rates for the fourth stage were calculated to be 25.15 radians per second at ignition and 43.4 radians per second just before burnout. Therefore, the design condition to be met was 43.4 radians per second at the end of the fourth-stage thrusting.

It should be mentioned that the 43.4 radians per second was considered to be conservative because the formula was developed for constant values of spin rate and moments of inertia whereas during the thrusting, the actual spin rate and moments of inertia were changing in such a way as to increase the required steady-state spin rate. Thus the transient-spin-rate requirement, which lags behind the steady-state value (in a time sense) would necessarily be less.

An extensive effort was made to evaluate the various means of obtaining the required spin rate. Three methods were considered: the use of a spin table between the third and fourth stages energized just before fourth-stage ignition by small spin rockets, that of spinning the combined empty third stage and loaded fourth stage by spin rockets just before separation of the third and fourth stages, and that of spinning the third and fourth stages together by canted fins on the third-stage Nike. It was decided from the standpoint of reliability to use the canted-fin method of spinning the third and fourth stages together. This choice also relieved certain apprehensions concerning the roll-resonance problem which is discussed later. At this time, wind-tunnel tests on a similar multistage missile-booster combination became available (ref. 4) which indicated that rolling downwash is about 100 percent or that the cant angle on the most rearward set of fins controls the rolling input to the entire vehicle. This result appeared to be substantiated in a subsequent flight test. Thus, in the present test there was no need to counteract the canted fins on the third-stage Nike to prevent large rolling velocities while the first and/or second stages were attached. Rather than depend upon a need for a very accurate

prediction of spin rate developed, it was decided to design the fin cant to exceed the required spin rate. Third-stage Nike fins were canted 1° which was computed to result in a roll rate of about 54 radians per second at fourth-stage ignition - an excess of about 10 radians per second plus the amount of "spin-up" experienced as the 20-inch spherical rocket motor thrusted. This "spin-up" or amplification of the rolling velocity during thrusting is an effect of angular momentum conservation of the propellant and can result in large increases in spin rate. Reference 2 describes this effect and includes a chart which was used to estimate its magnitude for the spherical rocket motor used in the present investigation.

After these preliminary calculations, two other problems were recognized as requiring a more exact solution to the equations of motion. This was accomplished numerically with the IBM 704 electronic data processing machine.

The first of these problems was that of pitch-roll resonance. This is a condition in which motions about the flight path are amplified to a large extent when the rolling frequency becomes equal to the nutational frequency. (This resonant frequency $\sqrt{\frac{M_\alpha}{I_x - I}}$ is very nearly equal to the model nonrolling natural pitch frequency $\sqrt{-\frac{M_\alpha}{I}}$ for the slender configuration under consideration.) In the present investigation, roll rate was anticipated to be near zero from launching until separation of the second-stage Nike. At separation of the second stage, the third- and fourth-stage combination would start to spin, the spin rate increasing from near zero through the roll-resonance frequency to the steady-state value under existing conditions. Since even moderate angles of total yaw would result in large aerodynamic loads, it was necessary to check the model motions through resonance. The resultant pitch-yaw amplitude was computed (inputs to this simulation are listed in the next paragraph) and is shown in figure 10. Here the important result is that the maximum angular deviation of the vehicle from the flight path is seen to be 0.9°, an acceptably small value. This value was kept small by passing through the resonant frequency relatively quickly. It is interesting to note that passing through resonance very slowly would increase this deviation by a factor of about 10 and would probably result in structural failure of the vehicle.

The second problem requiring a machine solution can be called "exit instability." This is a condition experienced by vehicles exiting the atmosphere in which their oscillatory motions can grow larger and larger

due to a rapid decrease in atmospheric density. This type of instability is not uncommon and can occur whether or not the vehicle is spin stabilized. The possibility of exit instability in the present investigation was anticipated to occur for the most part during thrusting of the last stages where it would be masked or combined with the effects of variable inertias, spin rates, and so forth. Therefore, motions of the model from burnout and separation of the first-stage Nike to coasting of the burned-out last stage to an altitude of 320,000 feet were computed on the IBM 704 electronic data processing machine. Inputs to this simulation included:

(1) 1° cant of all third-stage Nike fins to produce roll (nominal fin cant angle)

(2) An assumed 0.2° cant of third-stage Nike fins in pitch plane

(3) An assumed 0.001 radian angular thrust asymmetry of third-stage Nike nozzle in yaw plane

(4) An assumed 0.001 radian angular thrust asymmetry of fourth-stage spherical rocket motor in the yaw plane

(5) An assumed zero angular deviation of geometric and principal axes for all stages.

Results of this simulation showed that angular deviations of the geometric longitudinal axis from the flight path for all stages were within 0.2° except during pitch-roll resonance and during the last-stage thrusting and coasting.

Figure 11 presents portions of the total yaw angle during last-stage thrusting. The complex wave form is due to the usual precessional and nutational modes plus the added effects of time varying mass, velocity, moments of inertia, spin rate, overturning moments, jet damping, and atmospheric density. Part (a), starting at ignition, shows a maximum total yaw of about $1\frac{1}{2}^{\circ}$. This value increases to slightly more than 2° about midway through the thrusting (part (b)). At this time jet damping effects become dominant and gradually attenuate the total yaw to a nearly steady value of 0.7° (part (c)). This motion is carried over to the subsequent coast period of the last stage during which the angular motion remains unchanged since the vehicle is essentially above the atmosphere and has only negligible external moments acting on it.

Figure 12 was prepared to show the measured rolling velocity developed by the canted fins of the third-stage Nike up to ignition of the spherical motor. Also shown are the predicted spin rates (one of the outputs of the computer program) based on estimated roll inertias, roll damping

values of 80-percent linearized theory (ref. 5), and steady-state rolling rates from the following expression reported in reference 6:

$$\left.\frac{pb}{2V}\right|_{\substack{\text{Steady}\\\text{state}}} = \frac{2(\text{fin cant angle})}{57.3}\,\frac{1 + 2(\text{fin taper ratio})}{1 + 3(\text{fin taper ratio})}$$

where

V velocity along flight path

b wing span

p rolling velocity

Note the good agreement in figure 12 up to burnout of the third stage at t = 38.7. During the subsequent coast period, predicted spin rates are about 20 percent greater than those measured. This result was disappointing since similarly calculated results (unpublished) for another configuration showed good agreement at all velocities and altitudes.

Telemetered Accelerations

Normal and transverse accelerations of the third stage were telemetered throughout the flight and were found to vary from zero to about 4g. (See fig. 13 for sample time history.) These accelerometer records were intended for monitoring gross effects of the motion and could not be analyzed because of the excess of variables involved. However, the very small trim accelerations recorded throughout the flight indicate that the various stages were well balanced dynamically.

REFERENCES

1. Thibodaux, Joseph G. Jr., Swain, Robert L., and Wright, George: Analytical and Experimental Studies of Spherical Solid-Propellant Rocket Motors. NACA RM L57G12a, 1957.

2. Martz, C. William, and Swain, Robert L.: Experimental and Analytical Study of Rolling-Velocity Amplification During the Thrusting Process for Two 10-Inch-Diameter Spherical Rocket Motors in Free Flight. NASA TM X-75, 1959.

3. Anon.: Propellant Manual. SPIA/M2 (Contract NOrd 7386), Appl. Phys. Lab., The Johns Hopkins Univ., April 1959.

4. Gregory, Donald T., and Carraway, Ausley B.: Investigation of the Static Longitudinal Stability and Roll Characteristics of a Three-Stage Missile Configuration at Mach Numbers From 1.77 to 2.87. NASA TM X-124, 1959.

5. Piland, Robert O.: Summary of the Theoretical Lift, Damping-In-Roll, and Center-of-Pressure Characteristics of Various Wing Plan Forms at Supersonic Speeds. NACA TN 1977, 1949.

6. Strass, H. Kurt, and Marley, Edward T.: Rolling Effectiveness of All-Movable Wings at Small Angles of Incidence at Mach Numbers From 0.6 to 1.6. NACA RM L51H03, 1951.

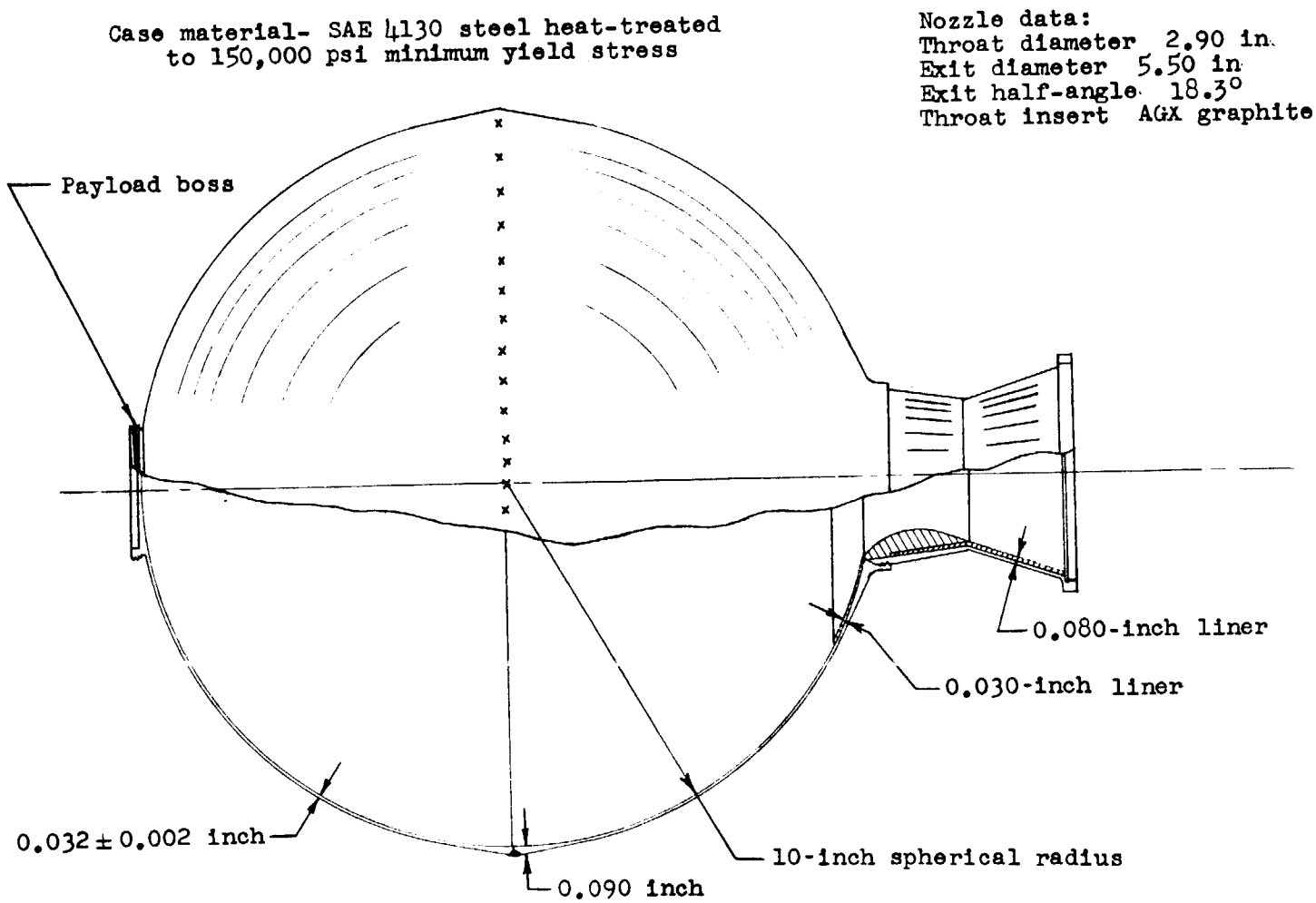

(a) 20-inch-diameter spherical rocket motor case and nozzle.

Figure 1.- Test model.

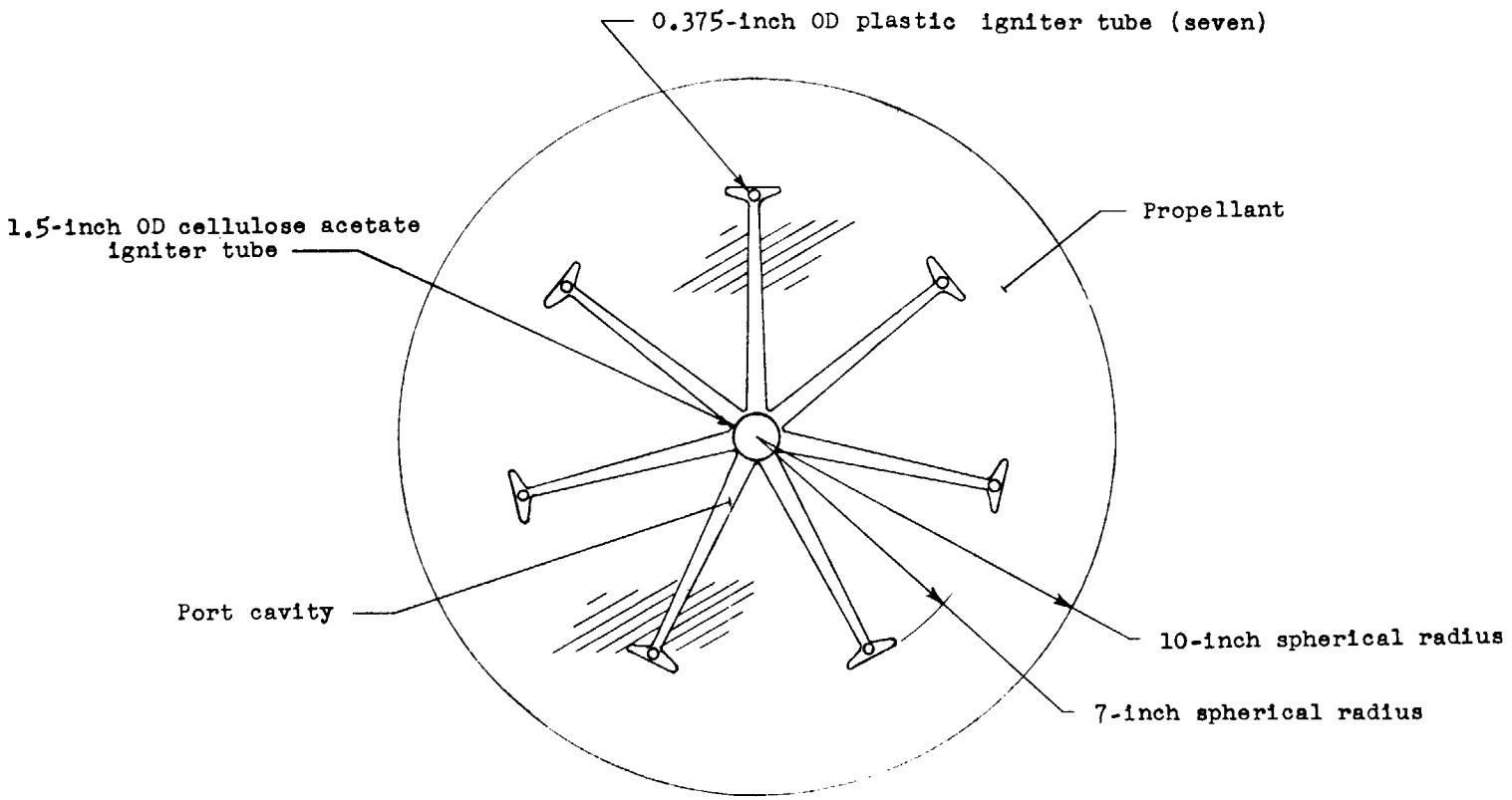

(b) Propellant configuration showing igniter location; cross-sectional view. (Section A-A on figure 1(c).)

Figure 1.- Continued.

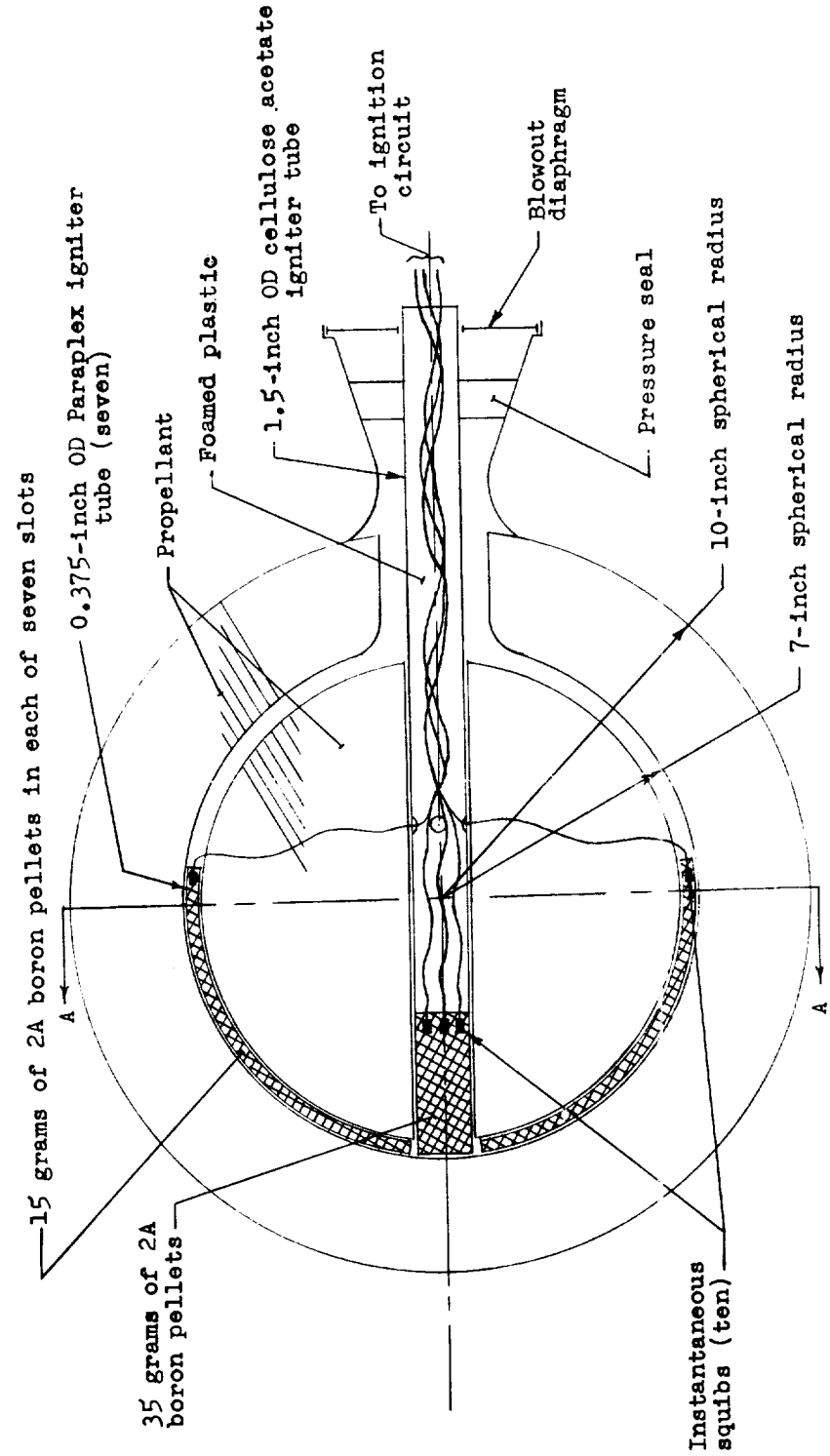

(c) Propellant configuration showing igniter location; side view.

Figure 1.- Continued.

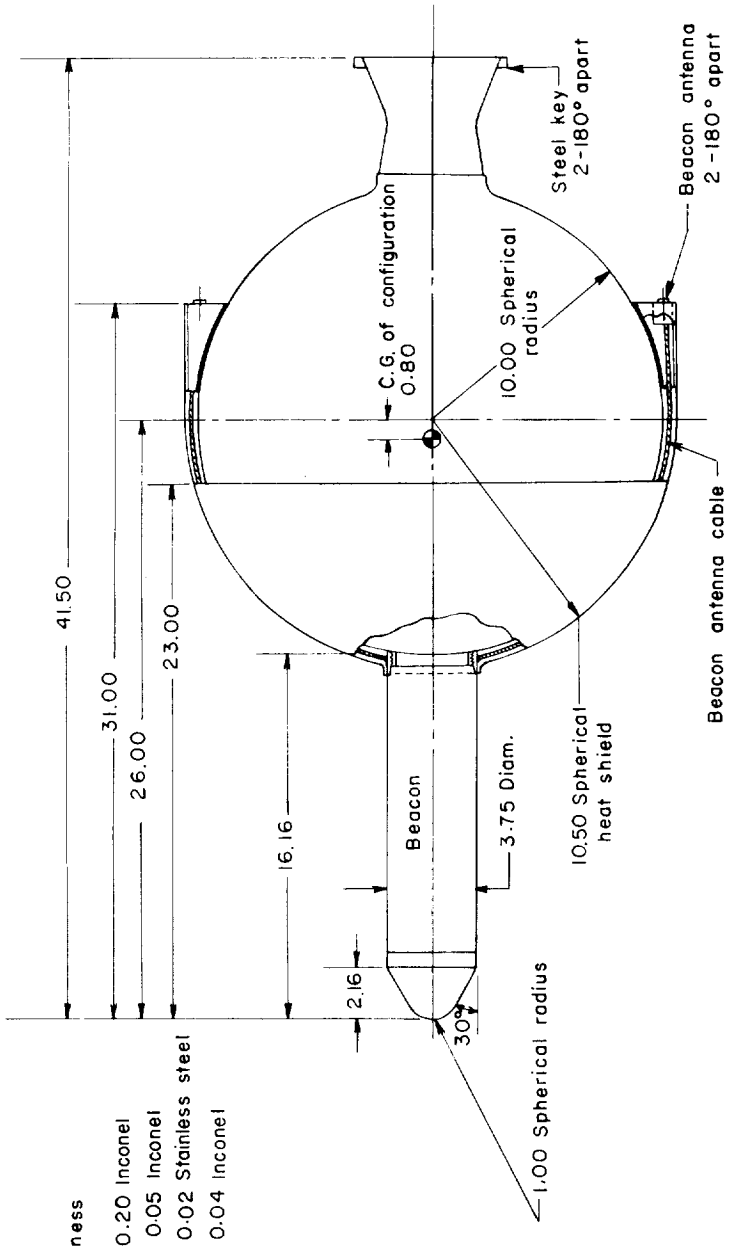

(d) General configuration. All dimensions are in inches.

Figure 1.- Continued.

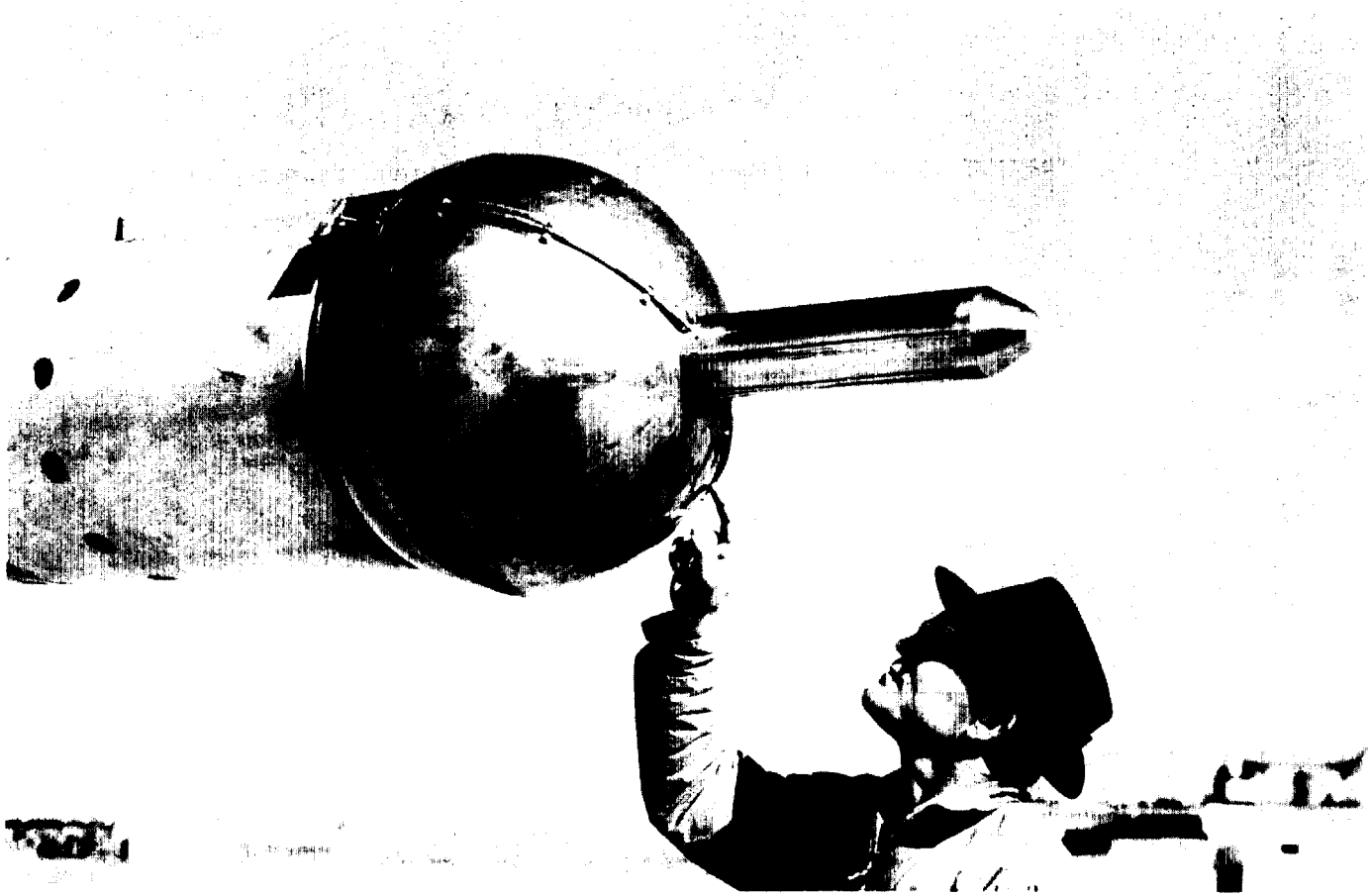

L-59-2121

(e) Photograph of spherical rocket motor with beacon assembly. (Heat shield removed.)

Figure 1.- Continued.

(f) Photograph of heat shield in position. L-59-2120

Figure 1.- Concluded.

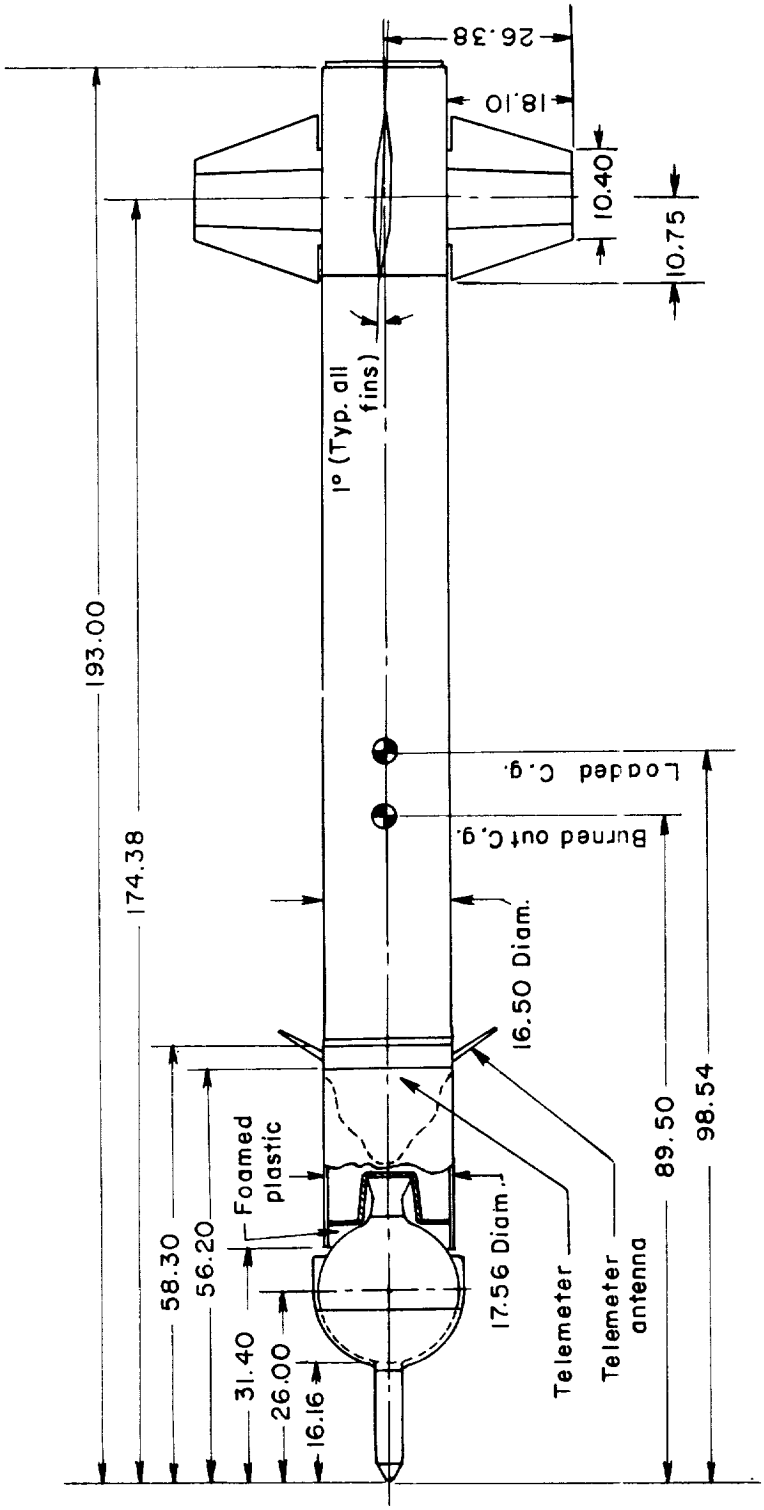

Figure 2.- Sketch of spherical rocket motor mounted to booster.

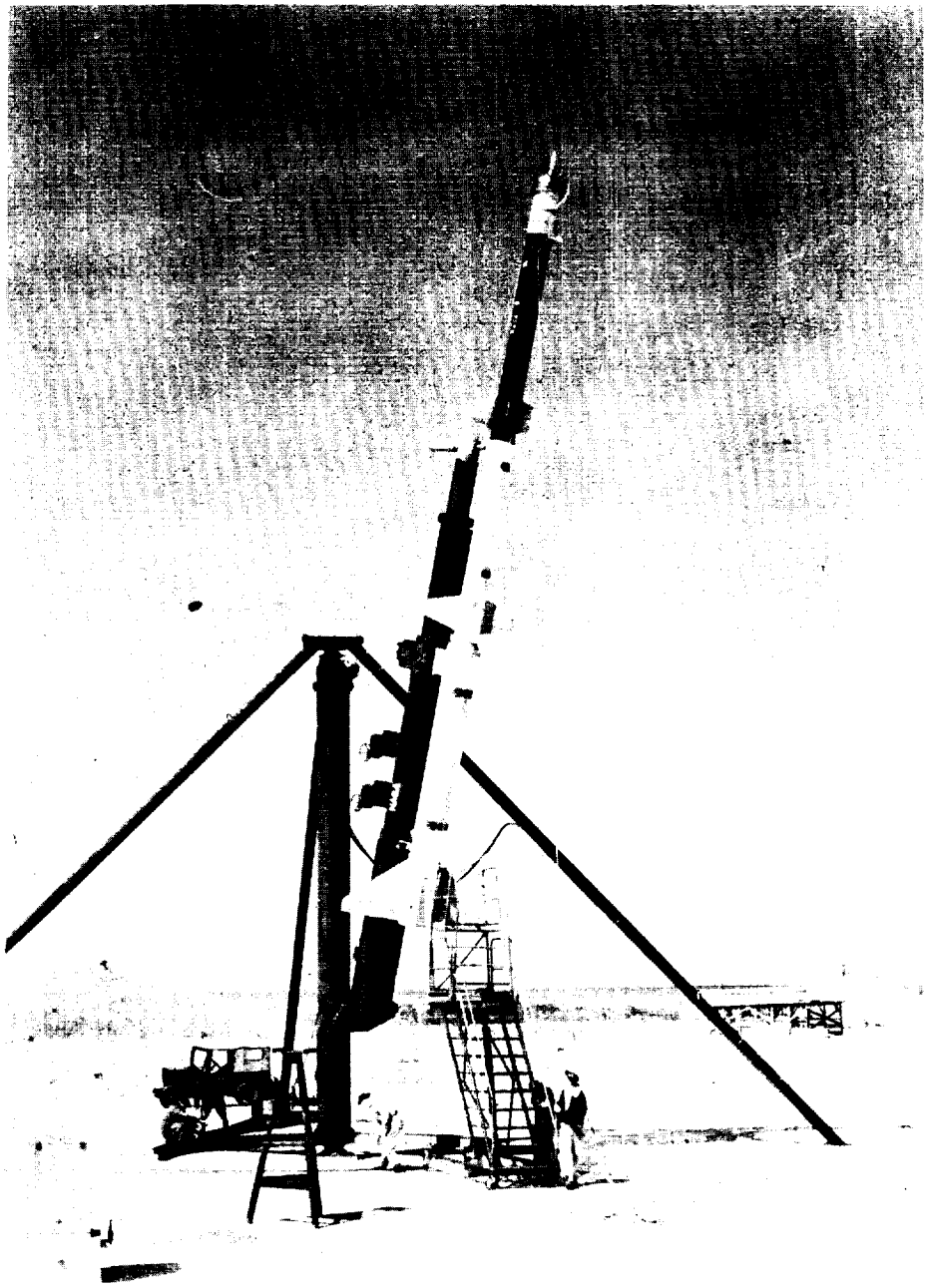

L-59-2122

Figure 3.- Photograph of spherical rocket motor and three booster stages on launcher.

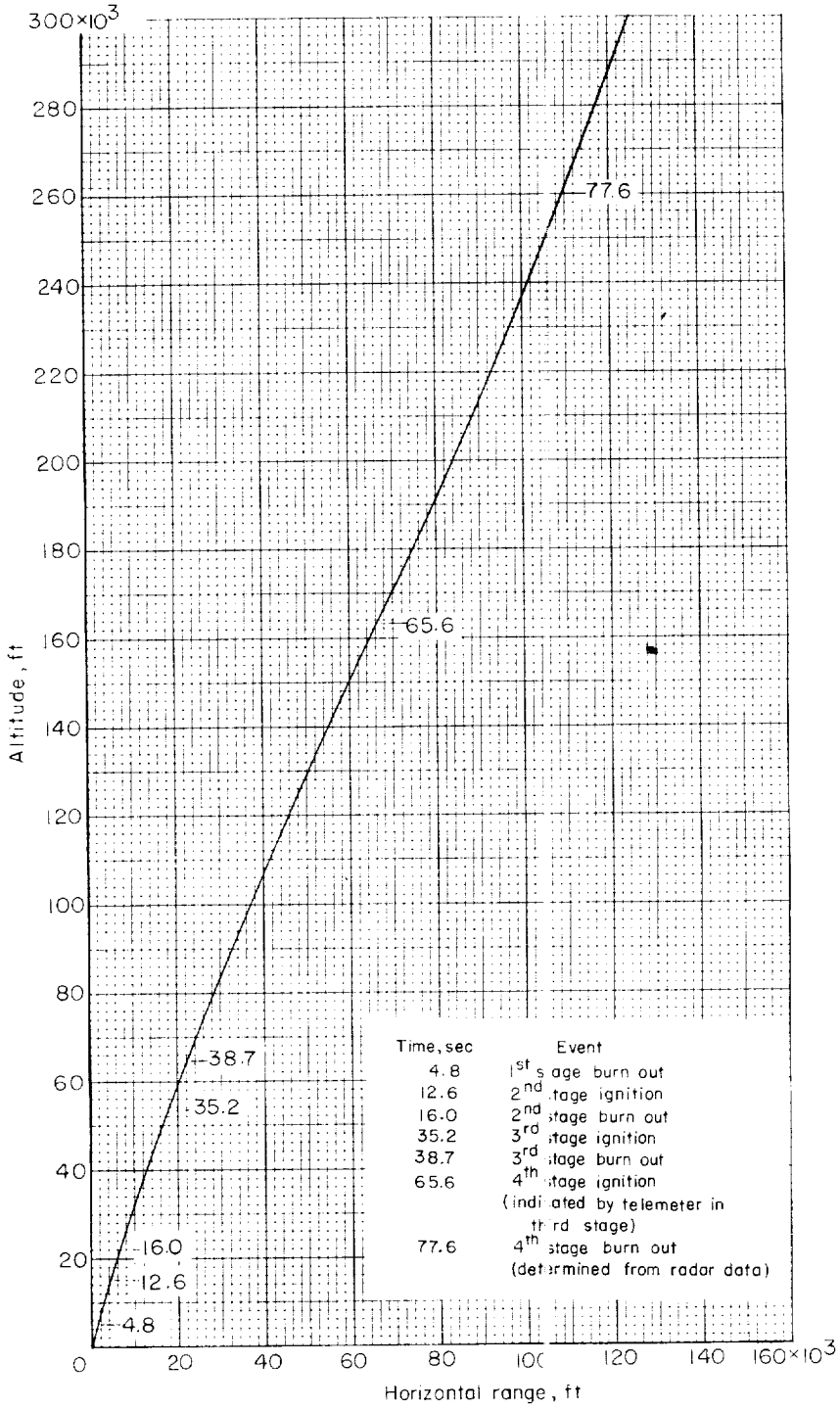

Figure 4.- Flight trajectory of test vehicle through sphere burnout.

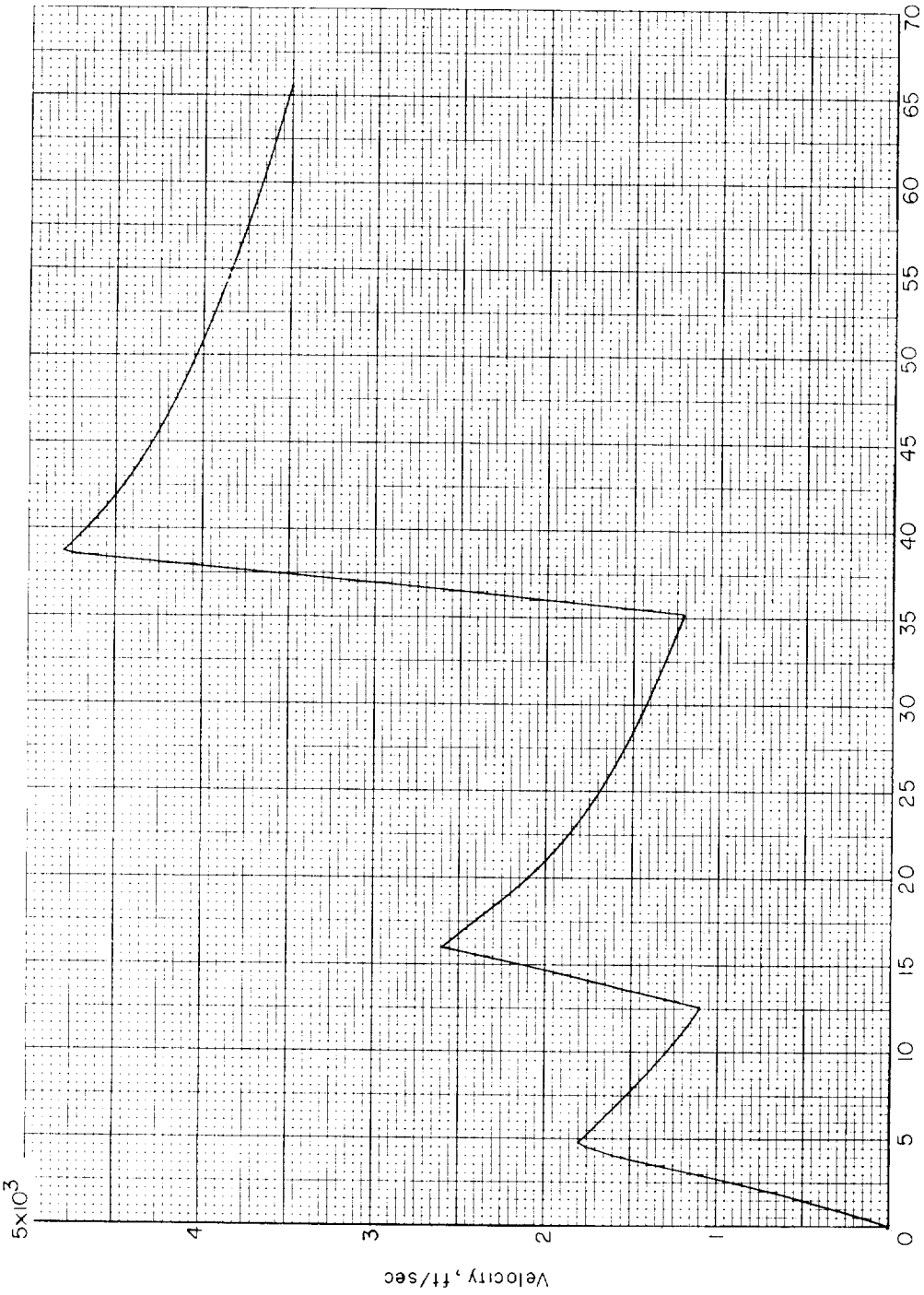

(a) 0 to 65.6 seconds.

Figure 5.- Time history of flight velocity.

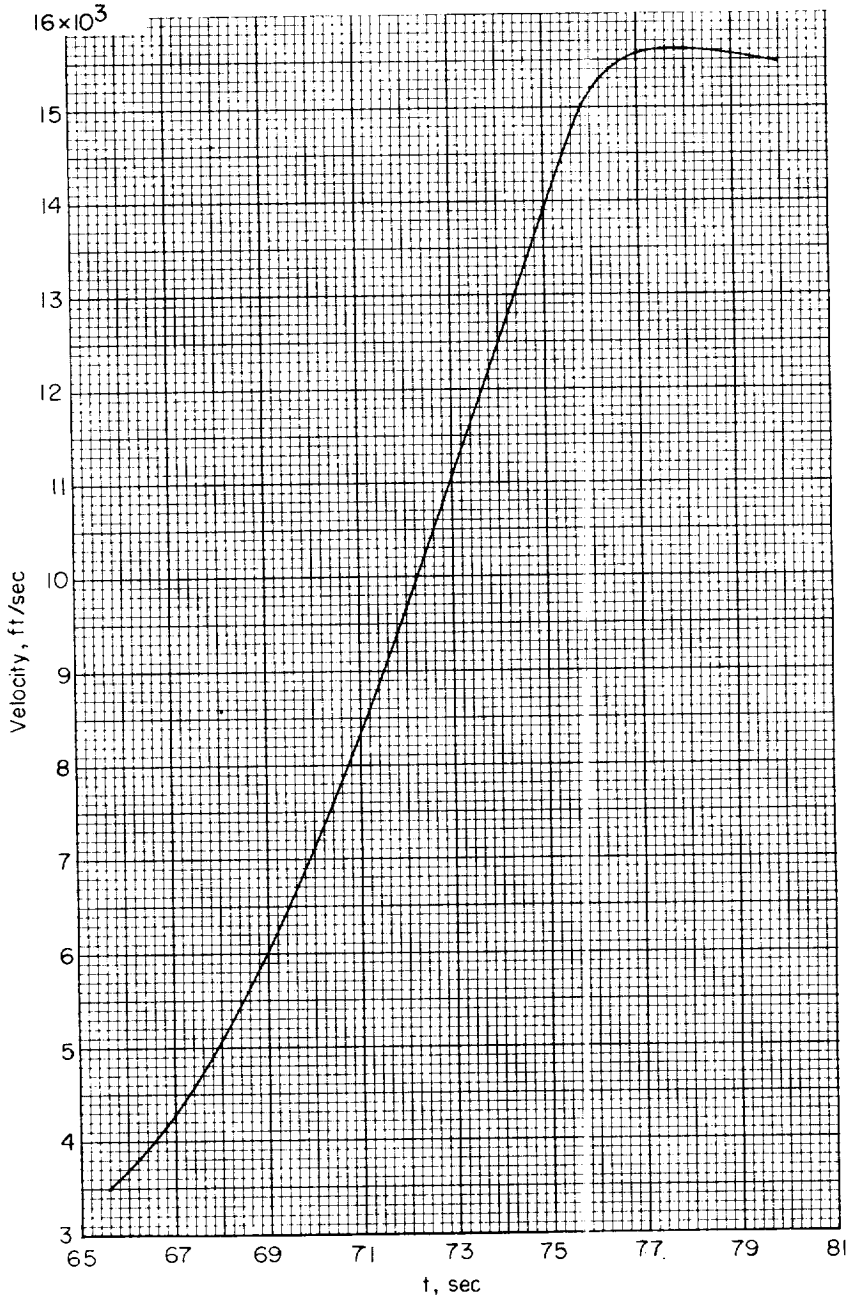

(b) 65.6 to 80.0 seconds.

Figure 5.- Concluded.

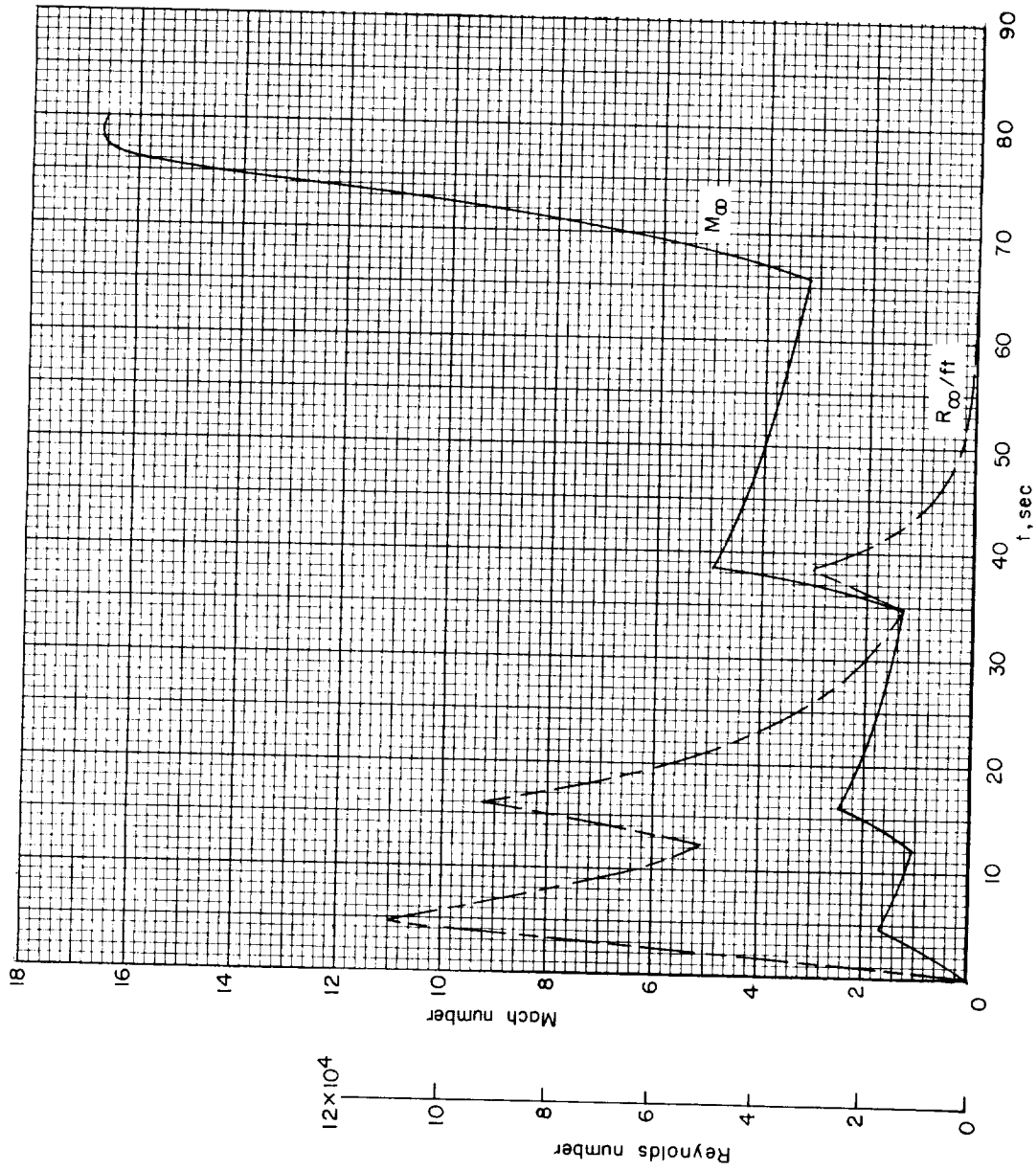

Figure 6.- Time histories of free-stream Mach number and Reynolds number per foot.

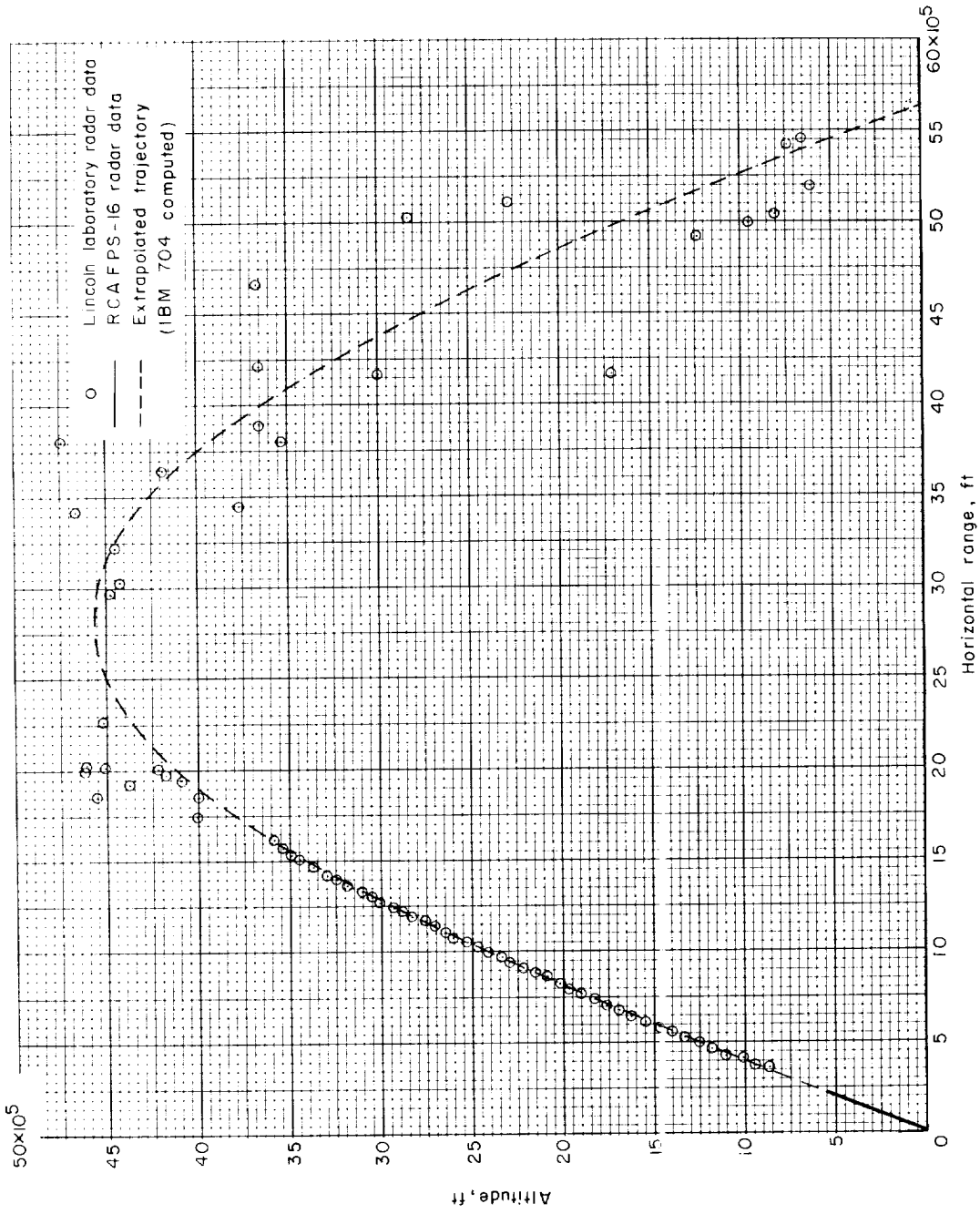

Figure 7.- Complete trajectory of spherical rocket motor.

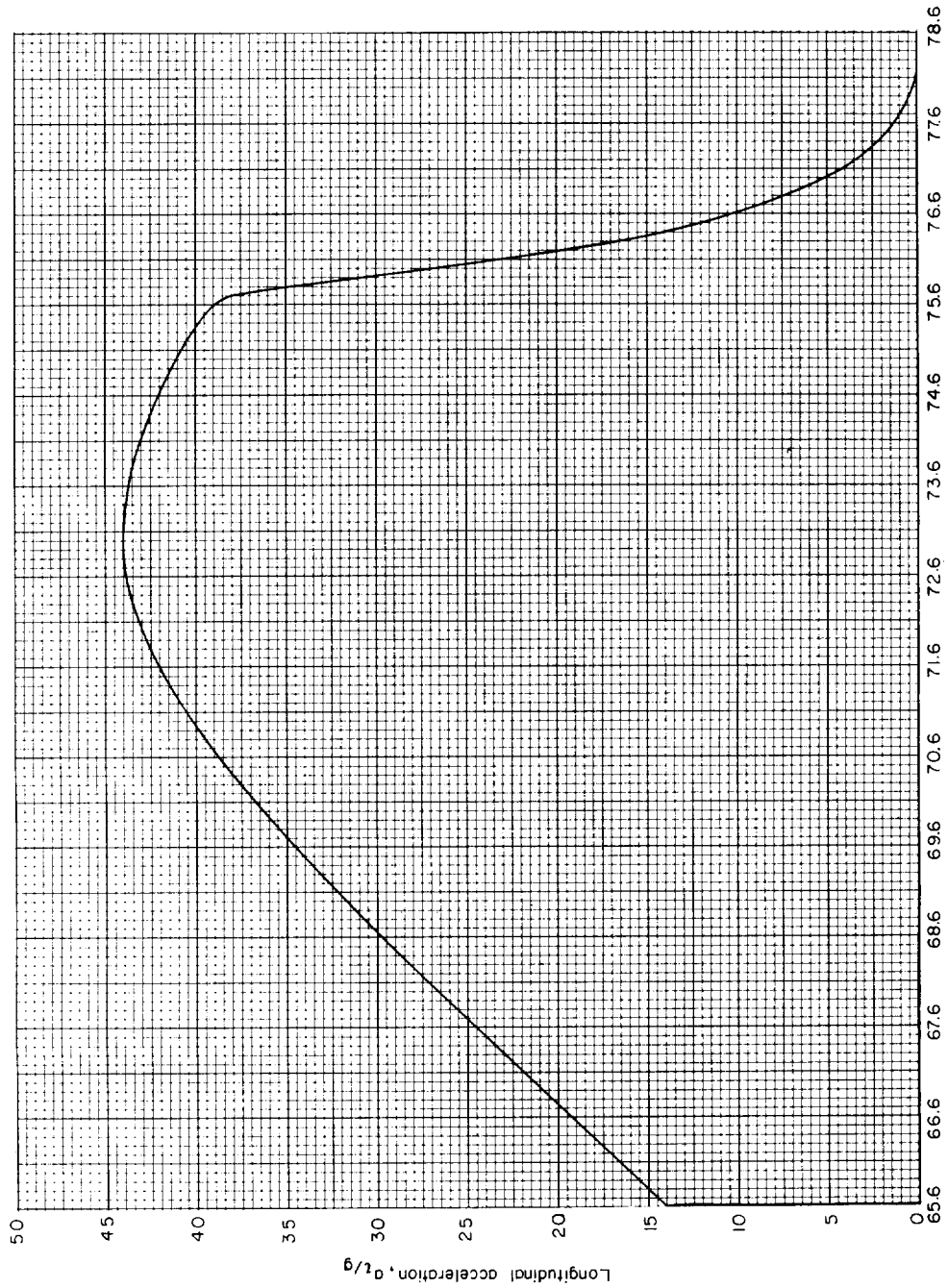

Figure 8.- Longitudinal acceleration during firing of the 20-inch-diameter spherical rocket motor as obtained from a differentiation of the velocity time history.

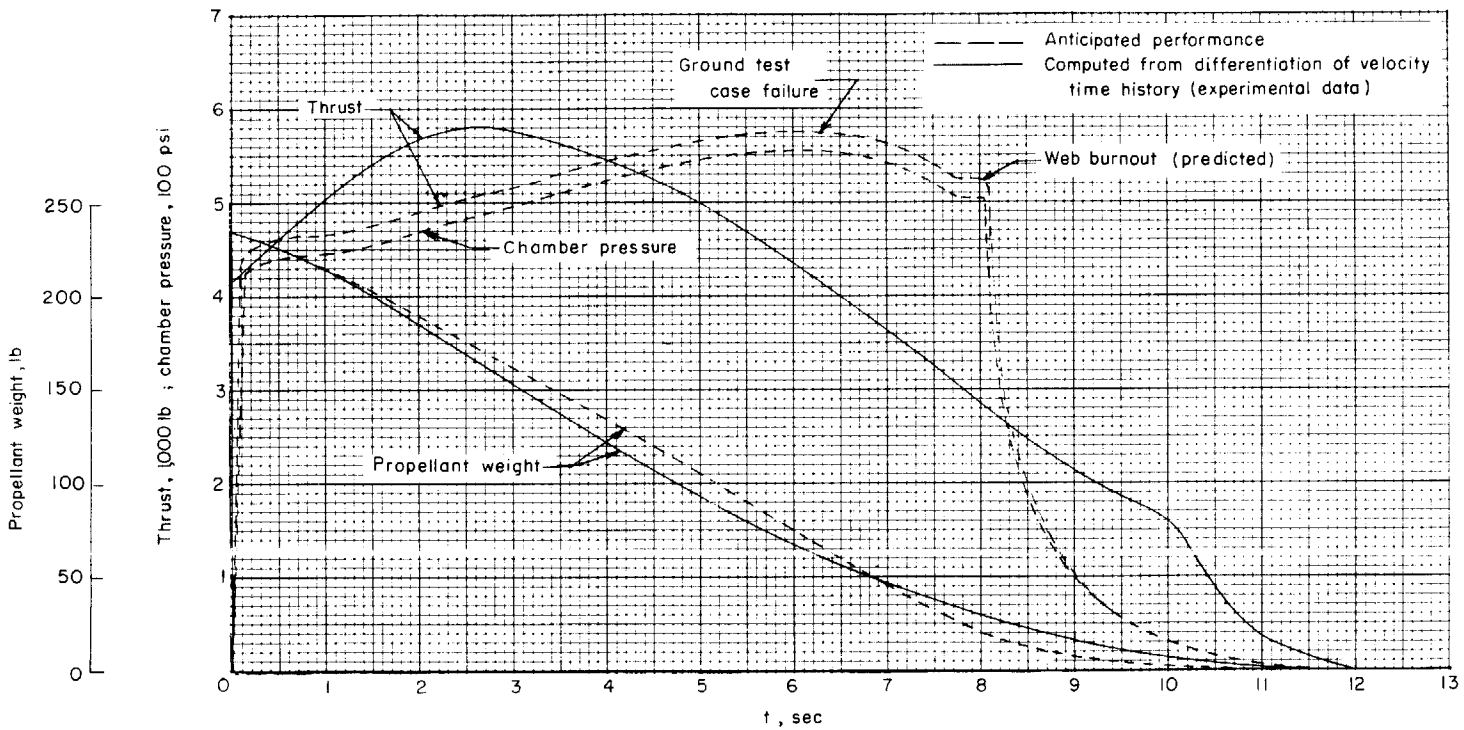

Figure 9.- Performance of a 20-inch-diameter spherical rocket motor.

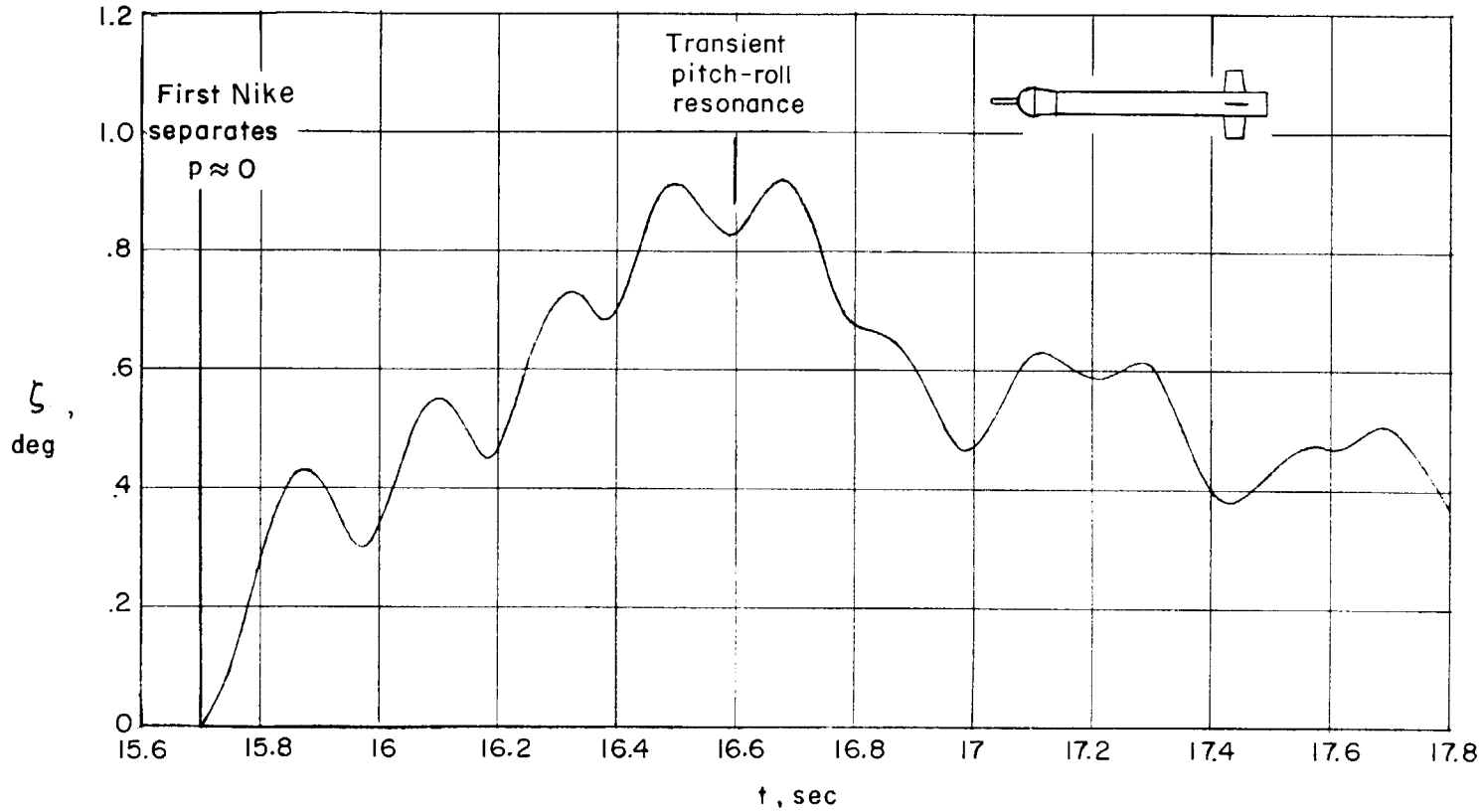

Figure 10.- Calculated history of complex yaw magnitude through pitch-roll resonance region for coasting model plus loaded third stage. Fin asymmetry 0.2° in pitch plane; initial altitude 23,000 feet.

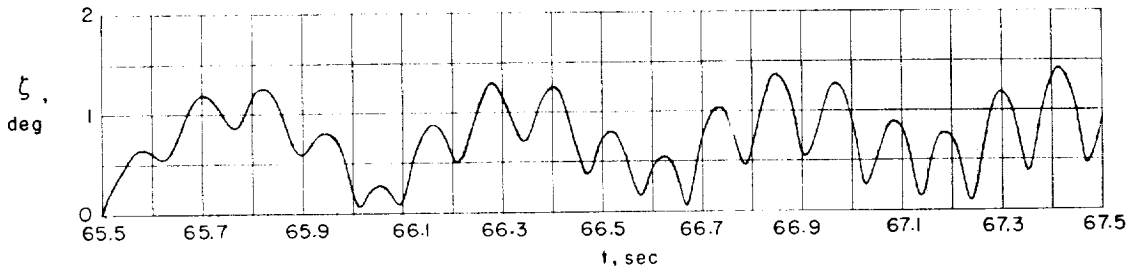

(a) Beginning of thrust period.

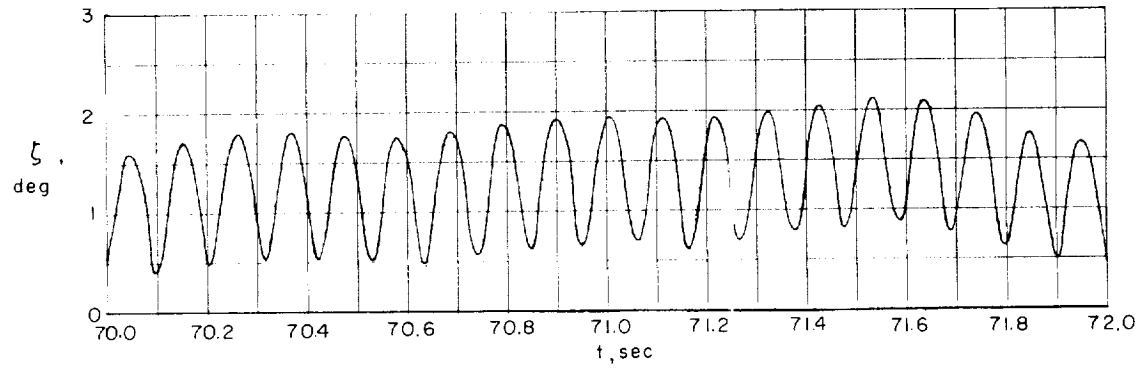

(b) Middle of thrust period.

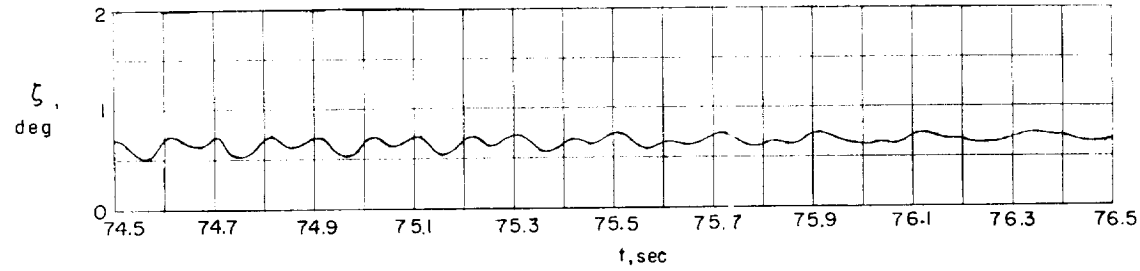

(c) End of thrust period.

Figure 11.- Calculated histories of complex yaw magnitude during thrusting of 20-inch-diameter spherical rocket motor.

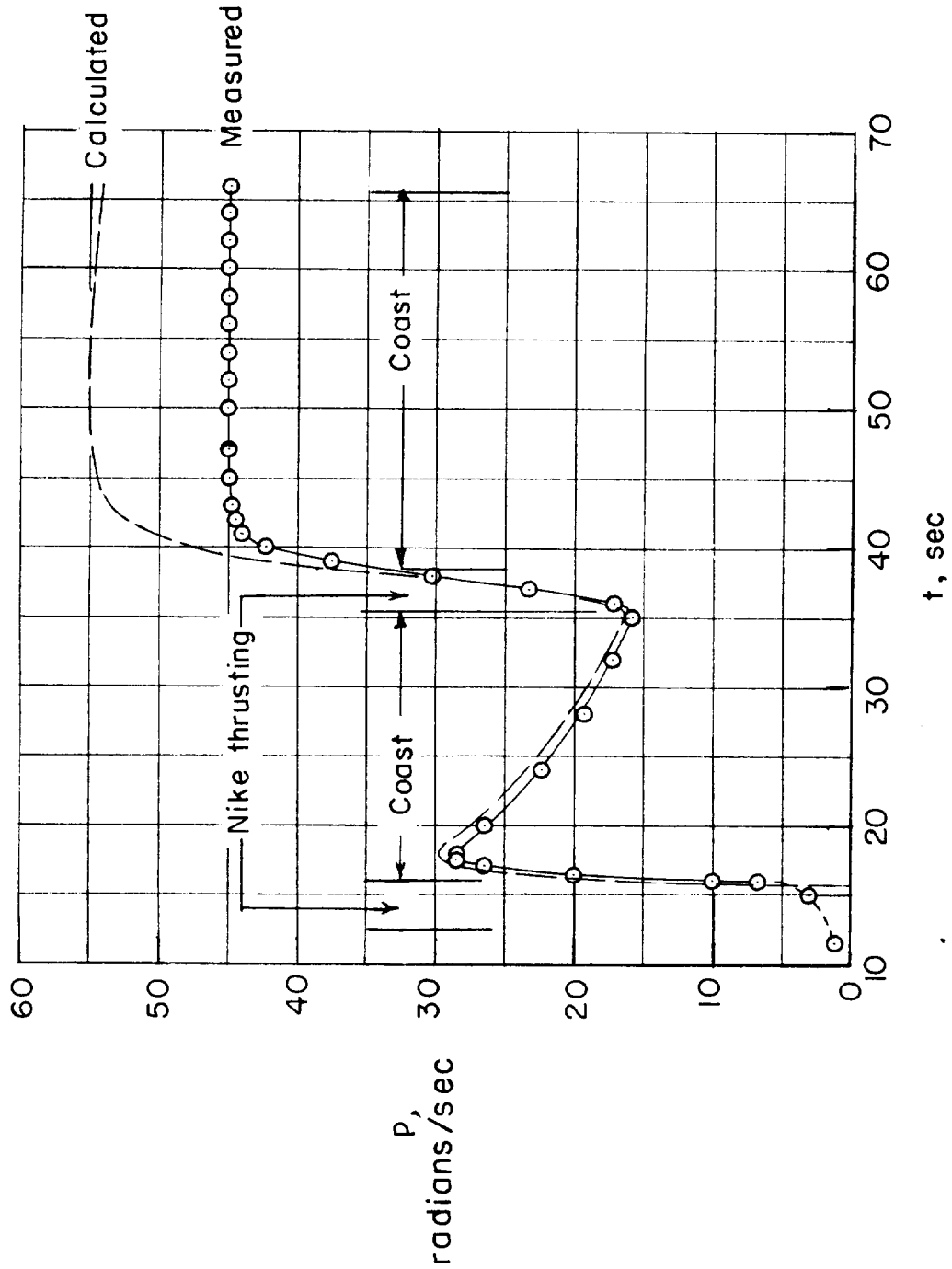

Figure 12.- Flight history of measured and calculated spin rates.

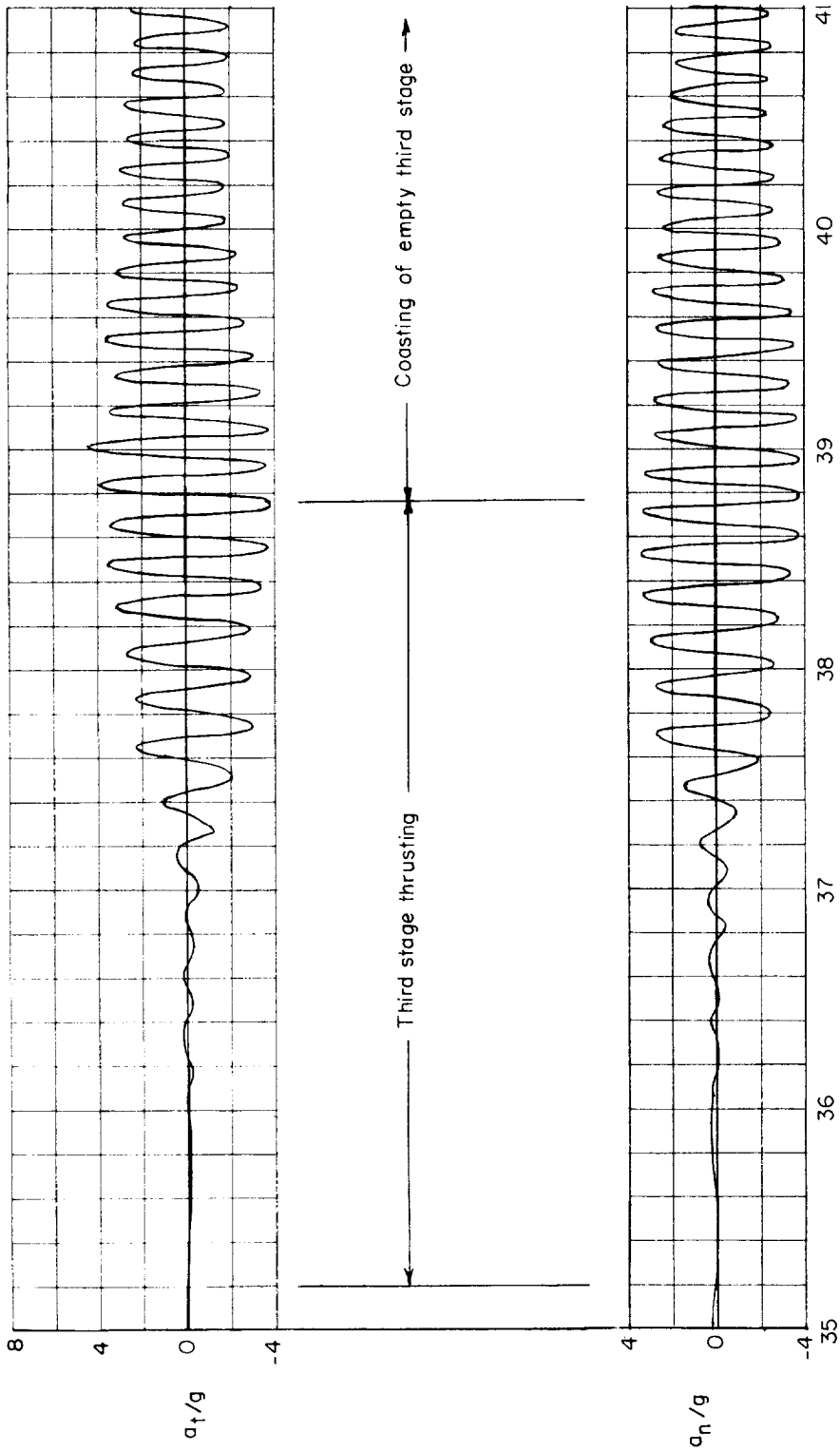

Figure 13.- Time history of measured normal and transverse accelerations of third stage.

NASA - Langley Field, Va. L-956